*Journal for ImmunoTherapy of Cancer*

# Bendamustine–rituximab elicits dual tumoricidal and immunomodulatory responses via cGAS–STING activation in diffuse large B-cell lymphoma

Ruipei Xiao [iD] ,[1,2] Wenli Zhao,[1] Wei Lin,[1] Yudian Xiao,[1] Jie Ren,[1] Yang Zhou,[1] Wei Meng,[1] Enguang Bi [iD] ,[1,3] Ling Jiang[4]

## ABSTRACT

**Background** Bendamustine–rituximab (BR) therapy stands out as a promising alternative for elderly patients with diffuse large B-cell lymphoma (DLBCL), demonstrating notable efficacy when conventional regimens pose challenges. Despite its clinical success, the intricate mechanisms underlying BR therapy have remained elusive.

**Methods** DLBCL cell lines were used to investigate the mechanism of BR therapy in vitro. RNA-seq and Western blot were used to explore the target pathways of BR therapy. STING was knocked out using Crispr-cas9 and inhibited using H-151 to investigate its role in BR therapy. Bulk RNA-seq and single-cell RNA-seq data from patients were analyzed to investigate the association between STING and pyroptosis pathways, validated using STING downregulated cells. Flow cytometry, transwell experiments and co-culture experiments were performed to investigate the inflammatory phenotype of DLBCL cells after BR treatment and its effect on T-cell recruitment and activation.

**Results** This study elucidates that BR elicits direct tumoricidal effects by promoting apoptosis and inducing cell cycle arrest. The synergistic impact with rituximab is further potentiated by complement addition, demonstrating the pivotal role of in vivo antibody-dependent cellular cytotoxicity. Moreover, our investigation reveals that, through a cGAS–STING-dependent pathway, prolonged exposure to BR induces pyroptosis in DLBCL cells. Activation of the cGAS–STING pathway by BR therapy triggers the release of inflammatory factors and upregulates major histocompatibility complex molecules, shaping an immunologically hot tumor microenvironment.

**Conclusions** This unique dual influence not only directly targets DLBCL cells but also engages the patient's immune system, paving the way for innovative combination therapies. The study provides comprehensive insights into the multifaceted actions of BR in DLBCL, offering a foundation for refined and personalized treatment strategies in elderly patients.

## WHAT IS ALREADY KNOWN ON THIS TOPIC

⇒ Bendamustine–rituximab (BR) therapy is recognized as a promising alternative for elderly patients with diffuse large B-cell lymphoma (DLBCL), although its intricate mechanisms have remained elusive.

## WHAT THIS STUDY ADDS

⇒ This study demonstrates that BR therapy elicits both tumoricidal and immunomodulatory responses through cGAS–STING activation in DLBCL.

## HOW THIS STUDY MIGHT AFFECT RESEARCH, PRACTICE OR POLICY

⇒ BR therapy shows potential as a complementary partner for immunotherapy, providing comprehensive insights for refining therapeutic strategies and personalizing treatment for DLBCL.

for 30%–40% of non-Hodgkin's B cell lymphomas (NHL) and manifesting an estimated annual global incidence of 150 000 cases.[1] The established first-line treatment for DLBCL is the immunochemotherapy regimen R-CHOP, which combines rituximab (anti-CD20 monoclonal antibody) with cyclophosphamide, doxorubicin, vincristine, and prednisone. This therapeutic regimen has demonstrated notable success, achieving a cure rate of over two-thirds of patients, thereby emphasizing the pivotal role of rituximab in the R-CHOP protocol.[2 3] However, a substantial challenge arises in treating patients with DLBCL aged over 70, who frequently present with additional medical conditions such as heart failure, thus rendering them intolerant to anthracycline or unable to adhere to planned doses and schedules due to associated toxicity.[4–6] Therefore, there is an urgent need to explore alternative, effective, and personalized therapeutic approaches.

Bendamustine, an alkylating agent synthesized in the 1960s that contains both alkylator

## INTRODUCTION

Diffuse large B-cell lymphoma (DLBCL) represents the predominant aggressive subtype among adult lymphomas, accounting

and a purine analog, is approved by USA FDA and the European Union for treating patients with chronic lymphocytic leukemia and indolent B-cell non-Hodgkin lymphoma.[7 8] It has demonstrated increased response rates and extended remission duration in patients with indolent B-cell lymphomas[9 10] and has proven effective and well-tolerated in cases of relapsed or primary resistant NHL.[11] Recent clinical studies have demonstrated a tolerability and favorable outcomes of bendamustine and rituximab (BR) therapy, especially in elderly patients with DLBCL and aggressive B-cell lymphoma.[11–13] Despite the promising efficacy of BR therapy in DLBCL treatment, the underlying molecular mechanism remains elusive.

As an alkylating agent, bendamustine mediates DNA cross-linking and damage, resulting in the generation of abnormal DNA in the cytosol.[14] Notably, the intracellular DNA receptor Cyclic GMP-AMP Synthase (cGAS) plays a crucial role in detecting aberrant double-stranded or single-stranded DNA fragments in the cytoplasm.[15 16] On sensing DNA abnormalities, cGAS initiates downstream signaling by translocating the signal to STING (Stimulator of Interferon Genes). Subsequent phosphorylation of STING activates TANK-Binding Kinase 1 (TBK1), triggering intrinsic immune signaling pathways, including the type I interferon signaling pathway and the release of interferons.[16–19] Targeting the cGAS–STING axis for inducing antitumor immune responses and enhancing the efficacy of immunotherapy represents a promising avenue in clinical trials. However, the role of STING in DLBCL and the impact of DLBCL therapies on STING activation remain inadequately understood.

In this study, we demonstrated that BR induces pyroptosis in DLBCL cells by activating the cGAS–STING pathway. This activation leads to the release of inflammatory factors, creating an immunologically hot tumor microenvironment. Additionally, BR therapy upregulates major histocompatibility complex (MHC) molecules on the tumor cell surface, enhancing T-cell activation and function. This study investigated the unique therapeutic mechanisms of BR in DLBCL treatment, providing insights for improved and personalized treatment options.

## METHODS AND MATERIALS
### Patient treatment and evaluation
We applicate bendamustine in combination with rituximab (BR) for the treatment of three patients with DLBCL who were unable to tolerate the CHOP regimen due to heart failure. Patients' information is included in online supplemental table 1. Four cycles of the BR regimen (bendamustine $100\,mg/m^2$ on days 1–2, rituximab $375\,mg/m^2$ on day 1, every 21 days) was applied, a follow-up PET-CT scans is used to evaluate the therapeutic effect of the tumor for all patients.

### Cell lines
The expression of CD20 (MS4A1) in DLBCL cell lines was analyzed with reference to published RNA-seq data GSE207388.[20] The CD20^{+} human DLBCL cell lines, OCI-LY1, KARPAS-422 and SU-DHL2 were grown in RPMI medium supplemented with 10% FBS (complement inactivated), 1% penicillin G/streptomycin. The 293 T-cell line used for gene transfection was grown in DMEM medium supplemented with 10% FBS, penicillin G/streptomycin. All cells were incubated at 37°C in a humidified chamber with 5% $CO_2$.

### STING KO cell line
To generate STING-KO OCI-LY1 cell line, a LentiCrispr v2 vector containing STING gRNA (Forward: CACC GGCGGGCCGACCGCATTTGGG, Reverse: AAACCCCA AATGCGGTCGGCCCGCC)[21] was used. Lentiviral supernatants were collected from a 293T packaging cell line transfected with the vector, packaging plasmids psPAX2 (Addgene #12260) and pVSV.G (Addgene #12259). Cancer cells were infected with the viral supernatants overnight in the presence of $10\,\mu g/mL$ polybrene and selected with $1\,\mu g/mL$ puromycin. Cells were tested repeatedly for mycoplasma over the course of the study and were never positive. The KO efficiency of STING was verified by western blot.

### Ubiquitination protease degrades STING in DLBCL cell line
SP23, a STING protein degrader based on a small-molecule STING inhibitor (C-170) and pomalidomide (a CRBN ligand),[22] was used to degrade STING protein in DLBCL cell line. DLBCL cell lines were pretreated with SP23 for 48 hours and then treated with BR or control in addition to SP23.

### Human STING inhibitor H-151 in DLBCL cell line
H151 (MedChemExpress, HY-112693), a STING inhibitor, was used to inhibit STING in DLBCL cell lines, with an equal volume of DMSO serving as the control. The DLBCL cell lines were treated with BR or the control, in addition to either H151 $(4\,\mu M)$ or DMSO.

### Human T cell
Peripheral blood mononuclear cells was isolated from donors' fresh blood using ficoll. MojoSort Human CD3^{+} T Cell Isolation Kit (Biolegend#480131) was used to isolate CD3^{+} T cell. Plate-bound anti-CD3 mAbs $(2\,\mu g/mL$, clone 17A2, eBioscience) and soluble anti-CD28 mAbs $(1\,\mu g/mL$, clone 37.51, eBioscience) may be used in some experiments to activate T cells. T cells were grown in OptiVitro T Cell Medium SF (TE000-N022) medium supplemented with IL-2 $(100\,U/mL)$.

### BR treatment in vitro
DLBCL cell lines were planted in 48-well culture plates at a concentration of $2\times10^5$ per well. B (bendamustine) group was treated the same as control group for 1 day before exposed to 200 µM bendamustine for 1.5 days. R (rituximab) group exposed to 10 µM rituximab for 2.5 days. BR (bendamustine+rituximab) group exposed to 10 µM rituximab for 1 day before exposed to 200 µM bendamustine and 10 µM rituximab for 1.5 days. The

control group was grown in the same culture conditions for 2.5 days without the addition of any drugs.

## Normal human serum treatment in vitro

The DLBCL cell lines were treated with normal human serum to mimic the cell growth environment that the complement is present in the patient. In the initial culture environment (RPMI medium supplemented with 10% complement inactivated FBS, 1% penicillin G/streptomycin), 5% more normal human serum (Solarbio#SL010) was added for the NHS (normal human serum) group. The condition of 65°C for 30 min was used to inactivate complement in normal human serum in order to obtain the inactivate complement normal human serum. In the initial culture environment, 5% extra inactivated complement normal human serum was added to the ICNHS (inactivate complement normal human serum) group.

## Cell viability assay

Annexin V -PI assay: DLBCL cell lines (SU-DHL2, KARPAS-422, OCI-LY1 and OCI-LY1 STING KO) were washed with PBS and resuspended in staining buffer containing Annexin V-APC (BioLegend), Annexin V binding buffer and PI (BioLegend). The percentage of live cells was determined by flow-cytometric analyses (Beckman) of Annexin V and PI double negative cells. The data were analyzed using FlowJo software.

CCK-8 assay: cell viability was determined with Cell Counting Kit-8 assay (APExBIO). Cells were plated in 96-well plates coated at a density of 5000 cells (SU-DHL2, KARPAS-422, OCI-LY1 and OCI-LY1 STING KO) for 48 hours. Next, 10 µL of CCK-8 was added to each well. The optical density was read at 450 nm using a microplate reader (FilterMax F5, Molecular Devices, USA) 3 hours later.

## Calculation of CI

In the same cell state, DLBCL cells were concurrently exposed to varying concentrations of rituximab (R) and bendamustine (B), as well as equivalent concentrations of the combination therapy (BR). Cell viability was assessed using the CCK8 assay. Referring to previous research,[23] the cell viability data and drug concentration data were input into the software Compusyn using the Non-Constant Ratio mode. The CI of R and B was then calculated automatically by the software. A CI value of less than 0.8 indicates that the two drugs exhibit synergism.

## Cell cycle assay

Flow cytometry was performed to analyze cell-cycle position. Cells were collected, rinsed and fixed in 70% ethanol for 12 hours in 4°C, and then washed again and resuspended in PBS solution containing Triton, RNase and propidium iodide. The samples were analyzed using a FACScan (Beckman).

## RNA sequencing (RNA-seq) and data analysis

From three replicates of OCI-LY1 cells of control group, R group, B group, BR group, total RNA was extracted from cells for RNA-seq using TRIzol reagent (Invitrogen; Thermo Fisher Scientific, Inc). RNA-seq was performed at Illumina Novaseq 6000 platform that included quality control, library preparation, fragmentation and PCR enrichment of target RNA according to standardized procedures. 150 bp paired-end raw reads were initially processed to obtain clean reads by removing adaptor sequences, low-quality sequences, and empty reads. After quality control, the clean reads were mapped to human genome (hg38) using HISAT software. Genes expression level were quantitated by FPKM (Fragments per kilobase of exon per million reads mapped). Between each two group, absolute log2FoldChange >1 and FDR significance score <0.05 were used as thresholds to identify DEGs. Volcano plots were generated using the R package EnhancedVolcano (V.1.12). Gene expression heatmap was drawn using R package pheatmap (V.1.0.12). The expression level is normalized by row. Enrichment analysis of DEGs between groups was performed using R packages clusterProfiler (V.4.2.2). GSEA was performed using R packages clusterProfiler (V.4.2.2) and GseaVis (V.0.0.2). Geneset was obtain from gene ontology (GO) dataset.

## Processing scRNA-seq data

Seven DLBCL samples from two public articles were download from GEO (https://www.nicbi.nlm.nih.gov/geo/, GSE182434) and heiDATA (https://heidata.uni-heidelberg.de/, VRJUNV).[24 25] After integration and removal of batch effect, a total of 26 844 single cells were obtained. The R package Seurat (V.4.3.0) was used to perform quality control (nFeature_RNA>600 & nFeature_RNA<3200 & percent.mt <10%) and normalization. In addition, genes detected in fewer than three cells were excluded. A total of 20 602 cells were used for following analysis. After scaling the expression matrix, principal component analysis (PCA) was then performed using RunPCA. RunHarmony was used to remove batch effects between different samples. T-SNE, UMAP visualization and SNN-based clustering were performed using the RunTSNE, RunUMAP and FindClusters functions within the Seurat package. Cell type annotation was performed using recognized marker genes: T cell (*CD3D, CD3E*), NK cell (*PRF1, NKG7*), B cell/Tumor (*CD19, CD79A, MS4A1*), Macrophage (*CD68*), Monocyte (*CD68, CD14, LYZ*). For B cells/tumor, we performed a second round PCA and UMAP reduction before they were divided into two groups (STING positive and STING negative) according to whether STING (TMEM173) was expressed. The expression levels of important proteins involved in pyroptosis (GSDMD, NLRP1, and CASP1) in these two groups were shown using DotPlot in Seurat. ssGSEA Score analysis of cGAS_STING and pyroptosis were performed using the AddModuleScore functions within the Seurat package. Geneset used for ssGSEA is shown in online supplemental table 2.

## Public tumor RNA-seq cohort of patients with DLBCL

RNA-seq data were downloaded from GDC and annotated with clinical message file[26] (https://gdc.cancer.gov/about-data/publications/DLBCL-2018).

### Survival analyses

Patients in the high expression group had gene expression levels in the top 50%, while those in the low expression group had gene expression levels in the bottom 50%. R packages survival (V.3.3-1) and survminer (V.0.4.9) were used for Kaplan-Meier overall survival analysis. Gene set score of each sample was calculated using R package GSVA (V.1.42.0). Parameters used are as follows: method= 'ssgsea', kcdf= 'Gaussian'. Gene set targeted by BR therapy: *CGAS, STING1, GSDMD, NLRP1, CASP1, IFNB1, TNF, CXCL10, HLA-A, HLA-B*, and *HLA-C*.

### Correlation analysis of gene expression

R package ggplot2 (V.3.36) was used to map correlation of gene expression levels in the form of FPKM. The method chosen was 'pearson'.

### Weighted gene coexpression network analysis

To identify coexpression gene clusters, R package WGCNA (V.1.72) was used to perform WGCNA.[27] Only the genes with variance not equal to 0 in all samples and missing values less than 10% were used to identify coexpressed gene clusters. Soft-thresholding power was determined as 10 using the scale-free topology principle. Correlation analysis was performed between results network modules and cGAS–STING-pyroptosis score (ssGSEA). The genes in the most correlated modules were extracted for further enrichment analysis (GO).

### T-cell infiltration level

R package MCPcounter (V.1.2.0) was used to analyse T-cell infiltration level.

## Protein–protein interactions

To analyze the possibility of protein interaction between STING and pyrogen-related proteins (GSDMD, NLRP1, CASP1), protein–protein interactions (PPIs) analysis was performed using the STRING database[28] (V.11.5, https://string-db.org/) with minimum interaction confidence of 0.4.

## Western blots and antibodies sources

Whole-cell extracts were prepared by lysing cells for 15 min on ice in RIPA lysis buffer (50 mM Tris-HCl (pH 7.5), 150 mM NaCl, 1.0% NP-40, 0.1% SDS and 0.1% Na-deoxycholic acid) supplemented with protease and phosphatase cocktail inhibitors (Thermo Fisher). Cellular lysates were assayed for protein concentration using Pierce BCA Protein Assay Kit (Thermo Scientific #23225) in 96 well-plates. Whole cell lysates were separated through SDS-polyacrylamide gels (8%–12%) and wet transferred to polyvinylidene di-fluoride membranes. Membranes were blocked with 5% milk powder in 0.1% Tween20 in 1x PBS (PBS-T) for 1 hour at room temperature followed by incubation with primary antibodies diluted in 2.5% milk PBS-T. Subsequently the membranes were incubated with secondary antibody conjugated with HRP and finally ECL (Millipore) was used to measure the protein bands semi-quantitatively and normalized to the gray value of GAPDH or β-actin. The following antibodies were used in this study: β-actin (CST#4967), CDKN1A (Abcam#ab107099), Bcl-2 (Biolegend#658701), Caspase-3 (Biolegend#634101), Caspase-8 (Biolegend#645501), cGAS (CST#15102), STING (zen-bioscience#300415), Phospho-STING (Ser366) (CST#50907), STAT1 (Biolegend#603702), Phospho-STAT1 (Ser727) (Biolegend#686402), GSDMD N-terminal (Immunoway#YT7991), and Caspase-1 (CST#2225).

## Quantitative real-time PCR (qRT-PCR)

cDNAs were synthesized from 2 μg of total RNA using the Hifair III first strand cDNA Synthesis SuperMix (YEASEN, 11137ES10). Real-time PCR was performed with Fast SYBR Green Master Mix (Vazyme, Q711-02) on the QuantStudio 3 applied biosystems (Thermo Fisher). The PCR primers used are as follows. CDKN1A F: 5′-TGTCCGTCAGAACCCATGC-3′, R: 5′-AAAG TCGAAGTTCCATCGCTC-3′, STING F: 5′-CCAGAGCA-CACTCTCCGGTA-3′, R: 5′-CGCATTTGGGAGGGAG TAGTA-3′, GAPDH: F: 5′-ACCCACTCCTCCACCTTTG-3′, R: 5′-CTCTTGTGCTCTTGCTGGG-3′, TNF: F: 5′-CTCT TCTGCCTGCTGCACTTTG-3′, R: 5′-ATGGGCTACAGG CTTGTCACTC-3′, IFNB1: F: 5′-CTTGGATTCCTACAAA GAAGCAGC-3′, R: 5′-TCCTCCTTCTGGAACTGCTGCA-3′, GSDMD: F: 5′-GTGTGTCAACCTGTCTATCAAGG-3′, R: 5′-CATGGCATCGTAGAAGTGGAAG-3′, NLRP1: F: 5′-CCACAACCCTCTGTCTACATTAC-3′, R: 5′-GCCC CATCTAACCCATGCTTC-3′, CASP1: F: 5′-GCTGAGGT TGACATCACAGGCA-3′, R: 5′-TGCTGTCAGAGGTCTT GTGCTC-3′. The relative amounts of PCR products generated from each primer set were determined on the basis of threshold cycle (Ct) using GAPDH as the loading control.

## Toxicity of bendamustine to T cells

T cells and OCI-LY1 cells were seeded in 48-well culture plates at a concentration of $2×10^5$ cells per well. They were treated with either C or B for 36 hours. Subsequently, both T cells and OCI-LY1 cells were harvested to assess cell viability using the Annexin V-PI assay. Additionally, in some wells, T cells were stimulated to assess the expression levels of IFN-γ, in order to evaluate the inhibitory effect of bendamustine on T cell response.

## T-cell transwell assay

Migration assays were carried out in 24-well culture plates using filters (5 μm pore size, CORNING Costar#3421). DMEM medium with 10% FBS was used as medium. Pretreated DLBCL cells (OCI-LY1, $2×10^5$) of C, R, B, and BR group were added to the lower compartment. $5×10^5$ activated human T cells were added on top of the insert. For C, R, B, BR group, the corresponding drug was

added to the medium. For BR wash group, OCI-LY1 cell was washed by PBS to remove BR and no additional BR is added to the medium. After incubation for 12 hours at 37°C, cells below the filters are collected and counted. They were labeled with CD4 and CD8 antibodies and analyzed by flow-cytometric (Beckman) and FlowJo software.

## Coculture of tumor and T cell

DLBCL cells from the C, R, B, and BR groups were cultured in OptiVitro T Cell Medium SF (TE000-N022) with the corresponding drugs for the drug pretreatment experiment. After pretreatment, the entire culture medium was collected for cell count. Then, 0.9 mL of the pretreatment medium (containing the drug) with $1\times10^5$ DLBCL cells was mixed with $3\times10^5$ activated T cells in 0.1 mL of fresh human T cell serum-free medium for co-culture. Additionally, 100 U/mL IL-2 was added to the medium. The mixture was then placed in a 24-well plate and incubated for 48 hours.

## Flow cytometry and antibodies

For surface staining, CD4 (APC, Biolegend, #300514), CD8 (APC-cy7, Biolegend, #344714), CD69 (Percp-cy5.5, Biolegend, #310926), TIM3 (PE-cy7, Biolegend, #345014), HLA-DR (PE-cy5.5, Biolegend, #307630), and HLA-ABC (APC, Biolegend, #311410) were used after Fc blocking. For intracellular staining of TNF-α (APC, BioLegend, 502912) and IFN-γ (PE, BioLegend, #383304), cells were stimulated in PMA (50 ng/mL; Sigma-Aldrich), ionomycin (500 ng/mL; Invitrogen), and brefeldin A (3 µg/mL; Sigma-Aldrich) for 4 hours. The result was analyzed by flow-cytometric (Beckman) and FlowJo software. The Fluorescence Minus One (FMO) control for each group was used to help define gating standard.

## Statistical analysis

Statistical parameters including sample size and statistical significance are reported in the figures and corresponding figure legends. In vitro comparisons of two groups of cells were made using the two-sided Student's t-test. Data are presented as means±SD and p≤0.05 was considered significant. Data were analyzed and plotted using GraphPad Prism V.9.3. **p<0.05; ***p<0.01; ***p<0.001; ****p<0.0001.

## RESULTS

## BR synergistically inhibit DLBCL tumors

To evaluate the efficacy of BR therapy, we administered the regimen to three elderly patients with germinal center B-cell (GCB) and activated B-cell (ABC) DLBCL who were intolerant to the R-CHOP regimen due to cardiac insufficiency (online supplemental table 1). Following four courses of BR treatment (bendamustine 100 mg/m² d1–2, rituximab 375 mg/m² d1, every 21 days as a course), all patients exhibited complete remission, as confirmed by the disappearance of tumor lesions on PET-CT scans (figure 1A). To investigate whether BR have a synergistic

killing effect on DLBCL cells, we selected both GCB and ABC DLBCL cell lines with CD20 expression (figure 1B). While bendamustine demonstrated dose-dependent cytotoxicity across three DLBCL cell lines, rituximab exhibited a similar minor killing effect within a concentration range of 5 µM to 40 µM (figure 1C, D and online supplemental figure S1A, B). Notably, rituximab significantly enhanced bendamustine's cytotoxicity (figure 1E and online supplemental figure S1C), and the synergistic effect of rituximab and bendamustine was verified by combination index (figure 1F, CI <0.8). Further investigations revealed that this synergistic effect was contingent on bendamustine concentration, not rituximab (online supplemental figure S1D, E). Given rituximab's known complement-dependent cytotoxicity in other B-cell lymphomas,[29 30] we explored its role in DLBCLs. The killing effect of rituximab combined with bendamustine was further heightened in the presence of normal human serum containing complement, while inactivated complement-containing serum showed no such enhancement (figure 1G, H, and online supplemental figure S1F). In the absence of complement when cultured with complement-inactivated fetal bovine serum, the direct killing effect induced by rituximab shown in figure 1D may be achieved by inducing apoptosis-related changes in mitochondria and mitochondrial membrane (online supplemental figure S1G). Concurrently, DLBCL cells exhibited a transition from early apoptosis to late necrosis between 12 and 36 hours of BR treatment (figure 1I).

## BR therapy blocks the cell cycle and induces apoptosis in DLBCL cells

To investigate the mechanism underlying the synergistic killing effect of BR therapy, we conducted RNA sequencing on OCI-LY1 cells treated with BR for 36 hours. Gene set enrichment analysis (GSEA) indicated a notable inhibition of the G1 to S phase transition of the cell cycle (figure 2A). Subsequent analysis revealed a significant upregulation of CDKN1A, the gene encoding the G1 cell cycle inhibitor P21, confirming the blockade of G1 cell cycle progression post-BR treatment (figure 2B–D). Time-course analyses unveiled an initial G2 phase arrest after 12 hours of BR treatment, shifting to a G1 phase blockade after 36 hours (figure 2E, F and online supplemental figure S2A). Additionally, BR treatment increased the percentage of cells in the subapoptotic phase, with the combination drug displaying superior efficacy compared with monotherapy (figure 2G, H and online supplemental figure S2B). Notably, expression of the antiapoptotic protein Bcl-2 decreased, while apoptosis-related proteins such as Caspase-3, Caspase-8, and Cleaved-Caspase-8 increased after 12 hours of BR therapy in OCI-LY1 cells (figure 2I).

## Activation of the cGAS–STING pathway by BR therapy

Analysis of differentially expressed genes in OCI-LY1 cells treated with BR therapy revealed significant alterations in pathways related to type I interferon and dsDNA response
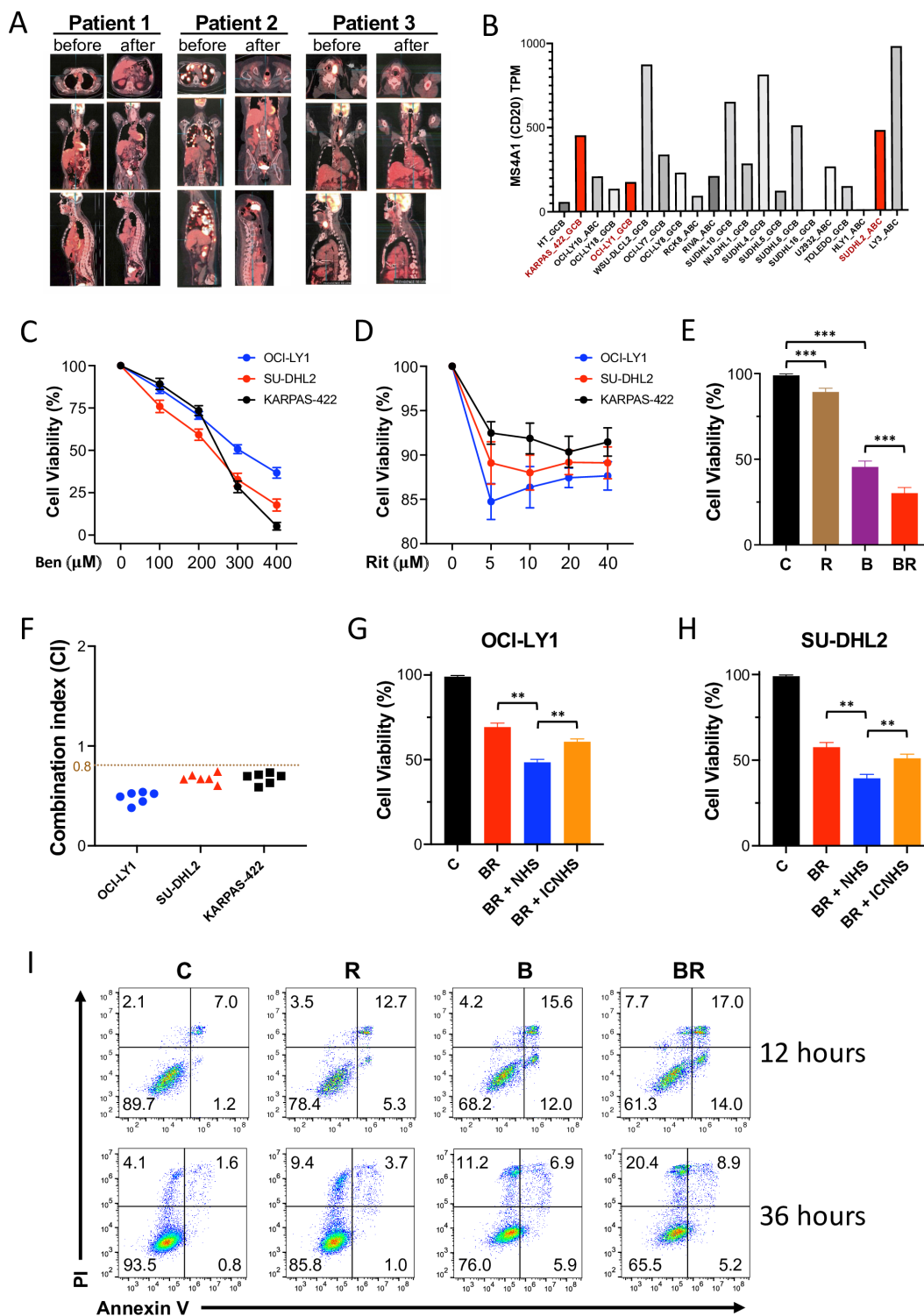
**Figure 1** Bendamustine and rituximab synergistically inhibit DLBCL tumors. (A) PET-CT images before and after four cycles of treatment for DLBCL. The left image displays the patient's pretreatment CT scan results, while the right image shows the post-treatment CT scan results. (B) CD20 expression in different DLBCL cell lines. The red color represents the cell lines selected for this study. (C, D) Cell viability assay. Cell viability of DLBCL cells (OCI-LY1, SU-DHL2, KARPAS-422) was assessed after treatment with different concentrations of bendamustine (C) or rituximab (D) for 36 hours. Cell viability: Annexin V-/PI- ratio of cells by flow cytometry. (E–H) Cell Counting Kit-8 assay for cell viability. (E) The viability of OCI-LY1 cells in C, R, B, and BR treatment group. (F) The CI of bendamustine and rituximab in three DLBCL cell lines. CI <0.8 indicates synergism. (G) The viability of OCI-LY1 cells in C, BR, BR+NHS, and BR+ICNHS group. (H) The viability of SU-DHL2 cells in C, BR, BR+NHS, and BR+ICNHS group. (I) Annexin-PI apoptosis assay. Percentage of apoptosis and necrosis in OCI-LY1 cells after treatment with C, R, B, and BR for 12/36 hours. B&Ben, bendamustine group; BR&Ben+Rit, bendamustine+rituximab; CI, combination index; C&CTRL, control group; DLBCL, diffuse large B-cell lymphoma; ICNHS, inactivated complement normal human serum; NHS, normal human serum; R&Rit, rituximab group. *p<0.05; **p<0.01; ***p<0.001; ****p<0.0001.
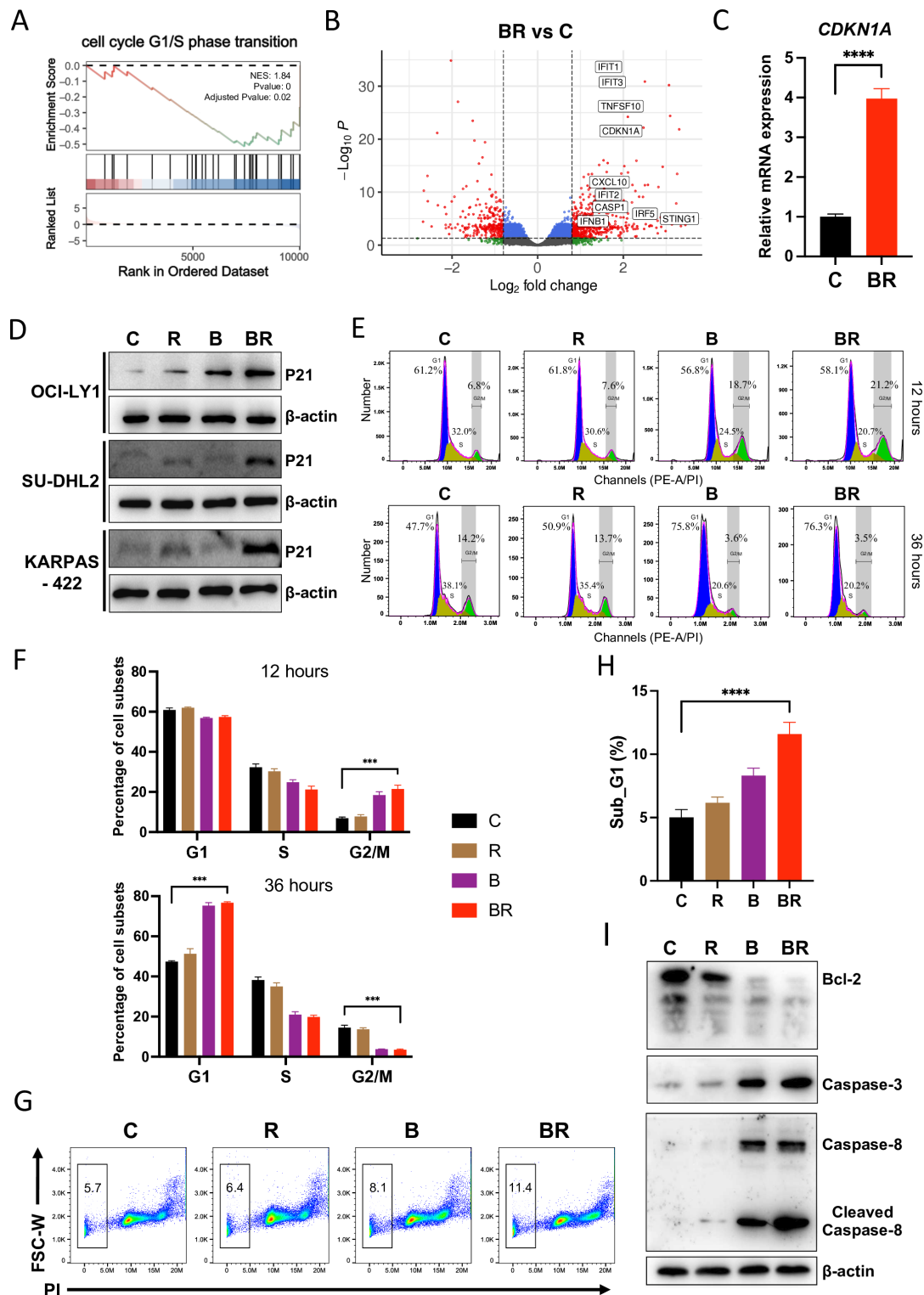
**Figure 2** BR therapy blocks the cell cycle and induces apoptosis in DLBCL cells. (A) GSEA based on BR treatment versus control dataset. (B). Volcano plot: volcano plot of differentially expressed genes in OCI-LY1 cells (BR vs control) using two-sided Wilcoxon rank-sum test. Log2FC cut-off: 0.8, p value cut-off: 0.05. (C) Assessment of CDKN1A expression by q-PCR. (D) Western blot analysis of P21 expression levels in three DLBCL cell lines in the C, R, B, and BR groups after 36 hours of treatment. β-actin was used as internal control. (E–F). PI flow cytometry staining to assess cell cycle status. Proportion of cell cycle at 12 hours (E upper and F upper) and 36 hours (E lower and F lower) after treatment with C, R, B, and BR in OCI-LY1 cell line. (G, H) Subapoptosis assay: (G and H) demonstrate subapoptotic status after 12 hours of C, R, B, and BR treatment. (I) Western blot analysis of Bcl-2, Caspase-3, Caspase-8, and Cleaved-Caspase-8 expression levels in OCI-LY1 cells after 12 hours of different treatments (C, R, B, and BR). β-actin was used as an internal control. B, bendamustine group; R, rituximab group; BR, bendamustine+rituximab; C, control group; DLBCL, diffuse large B-cell lymphoma; NES, normalized enrichment score; GSEA, gene set enrichment analysis. *p<0.05; **p<0.01; ***p<0.001; ****p<0.0001.

(figure 3A, B). Notably, genes associated with the cGAS–STING-Type I IFN signaling pathway were significantly upregulated following BR treatment (figure 3C, D). Since bendamustine can induce abnormal DNA fragments in the cytosol,[14] which cGAS can detect to initiate downstream signaling via the STING pathway, we investigated whether the cGAS–STING pathway is involved in the effects of BR therapy. Increased expression of cGAS and STING at both RNA and protein levels was verified in BR-treated cells, along with elevated phosphorylation of STING1 and STAT1 (online supplemental figure S3A, figure 3E–H). Though STING protein levels only increased in the early stage of BR treatment (20 hours, online supplemental figure S3A) but not in the later stage (36 hours, figure 3H). Increased phosphorylation of STING persists longer. It is reported that STING's steady-state regulation, involving ubiquitination and degradation, could contribute to the observed recovery in STING protein levels over time. This feedback mechanism helps prevent uncontrolled inflammatory responses.[31–34] We observed that genes involved in this negative feedback regulation were upregulated at 36 hours post-BR treatment (online supplemental figure S3B), which may account for the expression pattern of STING protein. Increased phosphorylation of STING was also obtained in SU-DHL2 cells (online supplemental figure S3C). Importantly, high STING1 expression in patients with DLBCL correlated positively with improved survival rates (figure 3I), which prompted us to explore the role of the cGAS–STING pathway in BR therapy's mechanism of action. To explore the relationship between BR-induced cytotoxicity and the cGAS–STING pathway, we performed CRISPR-Cas9-mediated STING1 knockout (KO) in DLBCL cell lines. Following puromycin selection, STING expression was dramatically downregulated, although not completely eliminated, likely due to incomplete KO in some cells (figure 3J). Downregulation of STING1 partial restored cell viability in OCI-LY1 and SU-DHL2 cells (figure 3K, L and online supplemental figure S3D, E). Further, the use of SP23, a STING1-specific ubiquitinated protease degrader, significantly decreased the cytotoxic effects of BR therapy (online supplemental figure S3F,G). Since the expression of STING was not completely eliminated by CRISPR/CAS9 in OCI-LY1 cells, a STING inhibitor H-151 was employed at maximum non-toxic concentration (4 µM, online supplemental figure S3H), which also led to significantly decreased cell death induced by BR therapy (figure 3M, N and online supplemental figure S3I, J). Collectively, these results emphasized the essential role of the cGAS–STING signaling pathway in BR-induced elimination of DLBCL cells.

### Activation of the cGAS–STING pathway induces pyroptosis in DLBCL cells by BR treatment

The RNA-seq analysis unveiled a significant increase in the expression of pyroptosis-associated genes, including pivotal players such as GSDMD, NLRP1 and CASP1, following BR treatment (figure 4A, B). This observation aligns with the identified PI mono-positive phenotype after 36 hours of BR treatment (figure 1I). Immuno-blot analyses showed heightened levels of GSDMD and Caspase-1 proteins (figure 4C), which validated the induction of pyroptosis.

The known association between the cGAS–STING pathway and pyroptosis prompted an exploration of their correlation in DLBCL cells.[35 36] Our analysis of the GDC-DLBCL-2018 cohort's RNA-seq data demonstrated a positive relationship between the expression of pyroptosis-related genes and STING1 (figure 4D). To strengthen this association, we integrated single-cell sequencing data, revealing distinct subpopulations (figure 4E, F). Remarkably, B cells expressing STING exhibited a notable upregulation of pyroptosis-associated genes (figure 4G). Further supporting this connection, ssGSEA analysis affirmed a colocalization of high scores for both the cGAS–STING and pyroptosis gene sets (figure 4H). The interaction network analysis illustrated a direct association between STING and pyroptosis proteins (figure 4I).

To reveal the relationship between upregulated STING and pyroptosis in DLBCL cells post-BR treatment, we detected the expression of pyroptosis-associated proteins in STING1-downregulated OCI-LY1 cells. The results demonstrated a significant reduction in the expression of pyroptosis-associated proteins (figure 4J). Similar results were observed with the STING inhibitor H-151 (figure 4K). All these results emphasized the pivotal role of the cGAS–STING pathway in promoting pyroptosis in DLBCL cells after BR treatment.

Above results clearly demonstrated that BR treatment blocks cell cycle to induce the early apoptosis and late pyroptosis by activating cGAS–STING pathway in DLBCL cells, which contributes to the direct toxicity of BR on DLBCL cells.

### BR-induced inflammatory microenvironment and T-cell infiltration

Since cGAS–STING pathway plays an important role in modulating adaptive immunity,[19] to understand the influence of the cGAS–STING pathway on the DLBCL tumor microenvironment, we performed Weighted Gene Co-Expression Network Analysis (WGCNA) on the GDC-DLBCL-2018 cohort. Two coexpression modules associated with cGAS–STING revealed significant enrichment in the TNF pathway, cytokines, chemokines, inflammatory response and T-cell activation pathways (figure 5A, B). Among these pathways, TNF is a crucial mediator that influences the inflammatory response within the tumor microenvironment.[37] To elucidate the origin of TNF, we analyzed single-cell RNA-seq data of DLBCL samples, and the results indicated B cells/tumor cells and T cells as primary sources of TNF within DLBCL samples (figure 5C). GSEA confirmed a significant enrichment of the 'TNF Signaling Pathway' in BR-treated DLBCL cells (figure 5D). Consistently, TNF expression was upregulated at both RNA and protein levels, along with increased expression of other inflammatory mediators and related
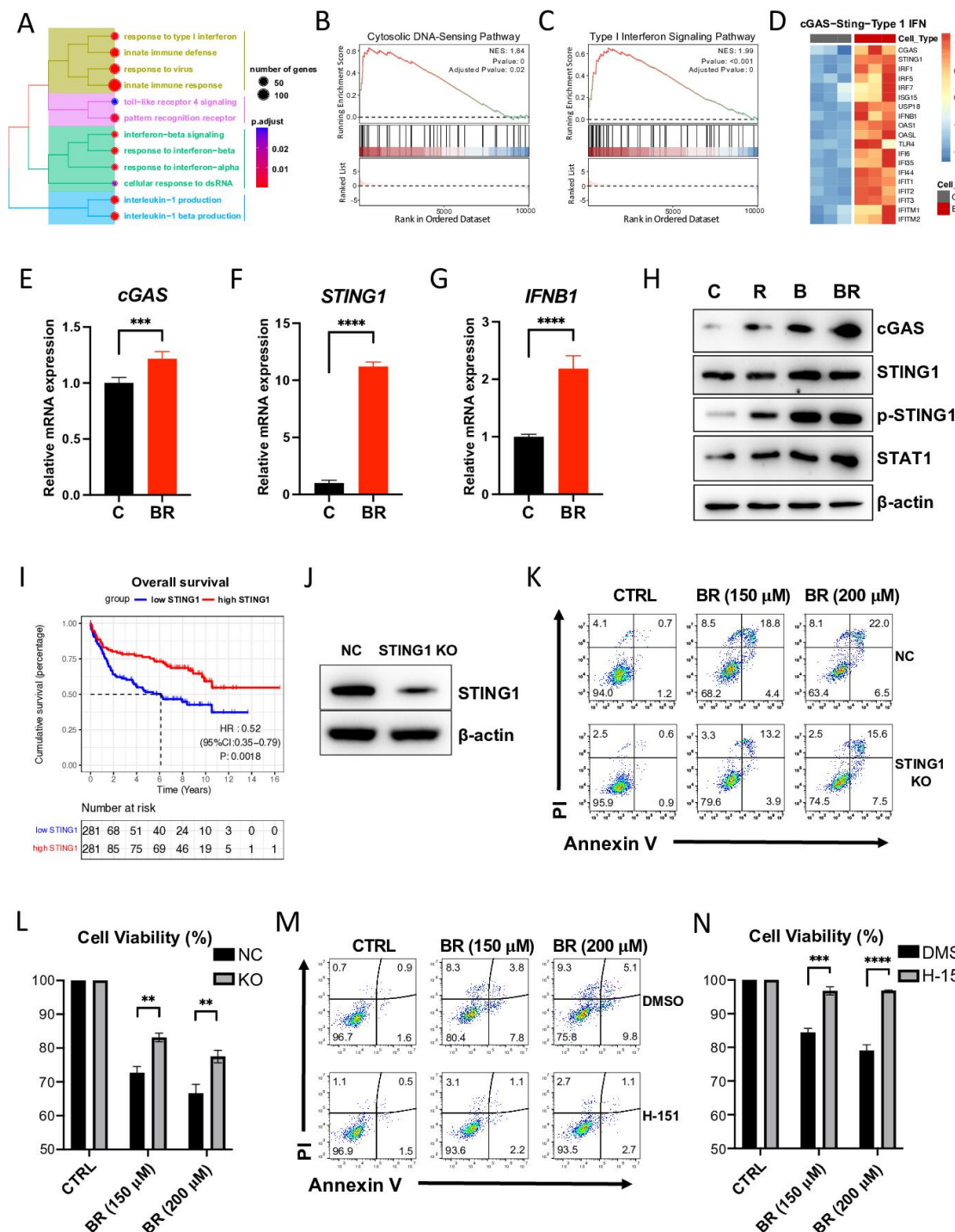
**Figure 3** Activation of the cGAS–STING pathway by BR therapy. (A) Gene pathway enrichment analysis in OCI-LY1 cells treated with BR versus C, based on the GO dataset. (B, C) GSEA results of OCI-LY1 cells treated with BR versus C. (D) Heatmap shows the variations in genes linked to the cGAS–STING-Type I IFN pathway in OCI-LY1 cells given BR or C treatment. (E–G) Gene expression was evaluated by RNA-seq (E) or q-PCR (F, G). (H) Western blot analysis was conducted to measure the expression levels of cGAS, STING1, p-STING1, and STAT1 in OCI-LY1 cells. The cells were exposed to various treatments (C, R, B, and BR) for 36 hours. β-actin was used as a control. (I) Kaplan-Meier (KM) survival curve displaying prognosis of high and low expression states of STING1. The p value was generated using the Mantel-Cox log-rank test. (J) Western blot analysis of STING1 expression levels in different groups (NC, STING1 KO) of OCI-LY1 cells. β-actin was used as a control. (K–N) Flow cytometric analysis was performed to measure the variance in levels of apoptosis between NC OCI-LY1 and STING1 KO OCI-LY1 (K) or between DMSO and H-151 treated OCI-LY1 cells (M), following 36 hours of BR treatment. The corresponding statistical results (L, N) were also obtained. NC: OCI-LY1 with empty vector, STING1 KO: STING1 Knockout OCI-LY1, C: control group, R: rituximab group, B: bendamustine group, BR: bendamustine+rituximab. CTRL: Control group, BR (150 μM): bendamustine 150 μM plus rituximab 10 μM, BR (200 μM): bendamustine 200 μM plus rituximab 10 μM. *p<0.05; **p<0.01; ***p<0.001; ****p<0.0001. GO, gene ontology; GSEA, gene set enrichment analysis.
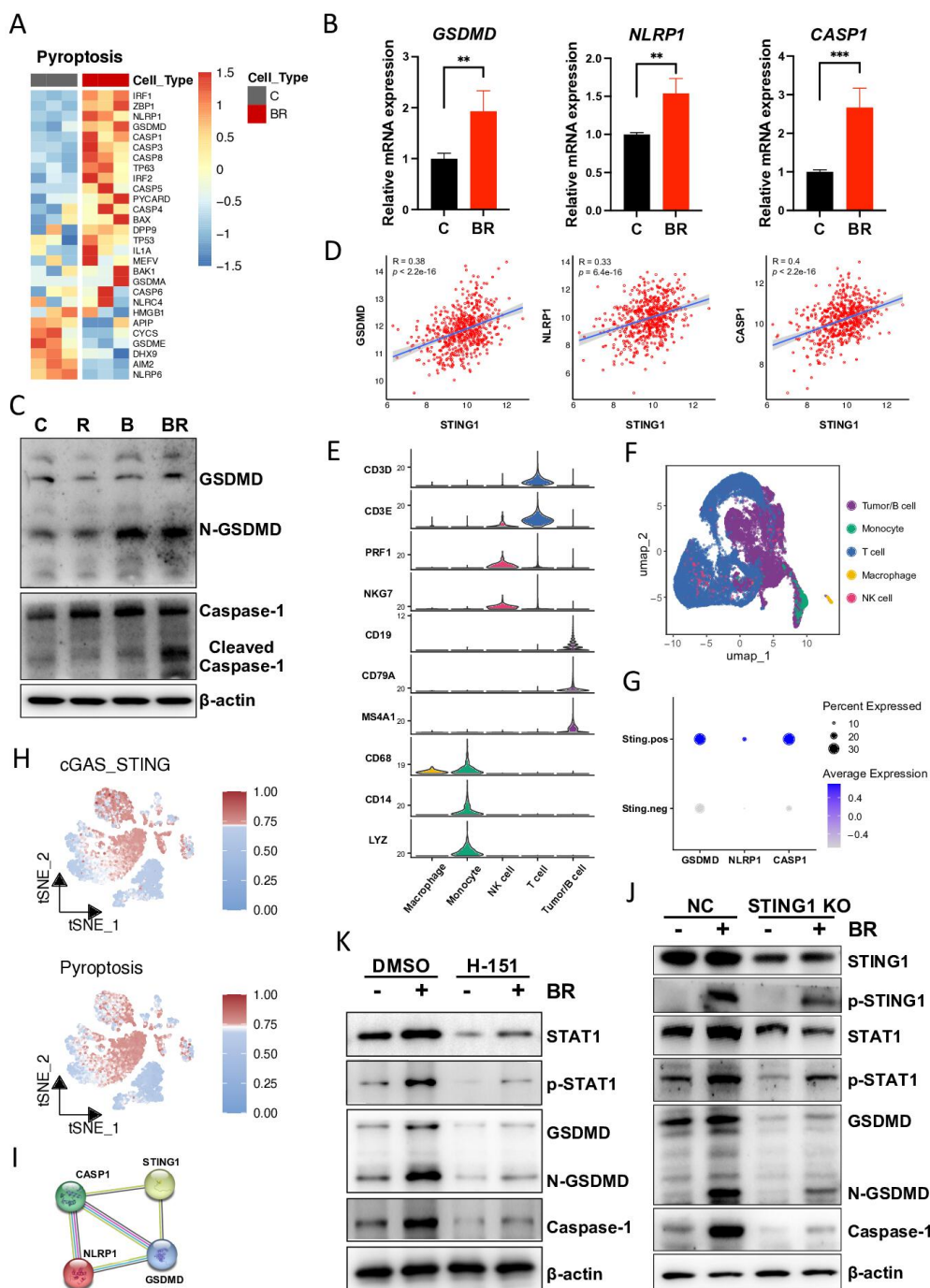
**Figure 4** Activation of the cGAS–STING pathway induces pyroptosis in DLBCL cells by BR treatment. (A) Heatmap displays the expression of genes related to pyroptosis in cells treated with BR compared with untreated OCI-LY1 cells. (B) Pyroptosis-related genes GSDMD, NLRP1, and CASP1 are measured using q-PCR. (C) Western blot shows the levels of GSDMD, N-GSDMD, Caspase-1, and Cleaved-Caspase-1 expressions in OCI-LY1 in different treatment group. β-actin used as a control. (D) Correlation analysis of pyroptosis-related genes GSDMD, NLRP1, and CASP1 with STING1 in TCGA-GDC dataset. R: Pearson Correlation Coefficient. (E) Violin plot shows marker genes used for cell annotation. (F) UMAP plot displays an overall cell annotation. (G) The expression level of pyroptosis-related genes (GSDMD, NLRP1, CASP1) in cells that either do or do not express STING in single-cell data. (H) Representation of cGAS_STING signatures and pyroptosis signatures in single-cell data of tumor/B cell. (I) A PPI network indicating the connection between STING and pyroptosis-related proteins GSDMD, NLRP1 and CASP1. (J) Western blot analysis to assess the expression of STING1, p-STING1, STAT1, p-STAT1, GSDMD, N-GSDMD, and Caspase-1 in NC and STING KO OCI-LY1. The analysis was conducted on both BR-treated and untreated groups. β-actin used as a control. (K) Western blot analysis to assess the expression of STAT1, p-STAT1, GSDMD, N-GSDMD, and Caspase-1 in DMSO and H-151 treated OCI-LY1 cell. The analysis was conducted on both BR-treated and untreated groups. β-actin used as a control. NC: OCI-LY1 with empty vector, STING1 KO: STING1 Knockout OCI-LY1, C: Control, R: rituximab, B: bendamustine, BR: Combination of bendamustine and rituximab therapy. *p<0.05; **p<0.01; ***p<0.001; ****p<0.0001. DLBCL, diffuse large B-cell lymphoma.
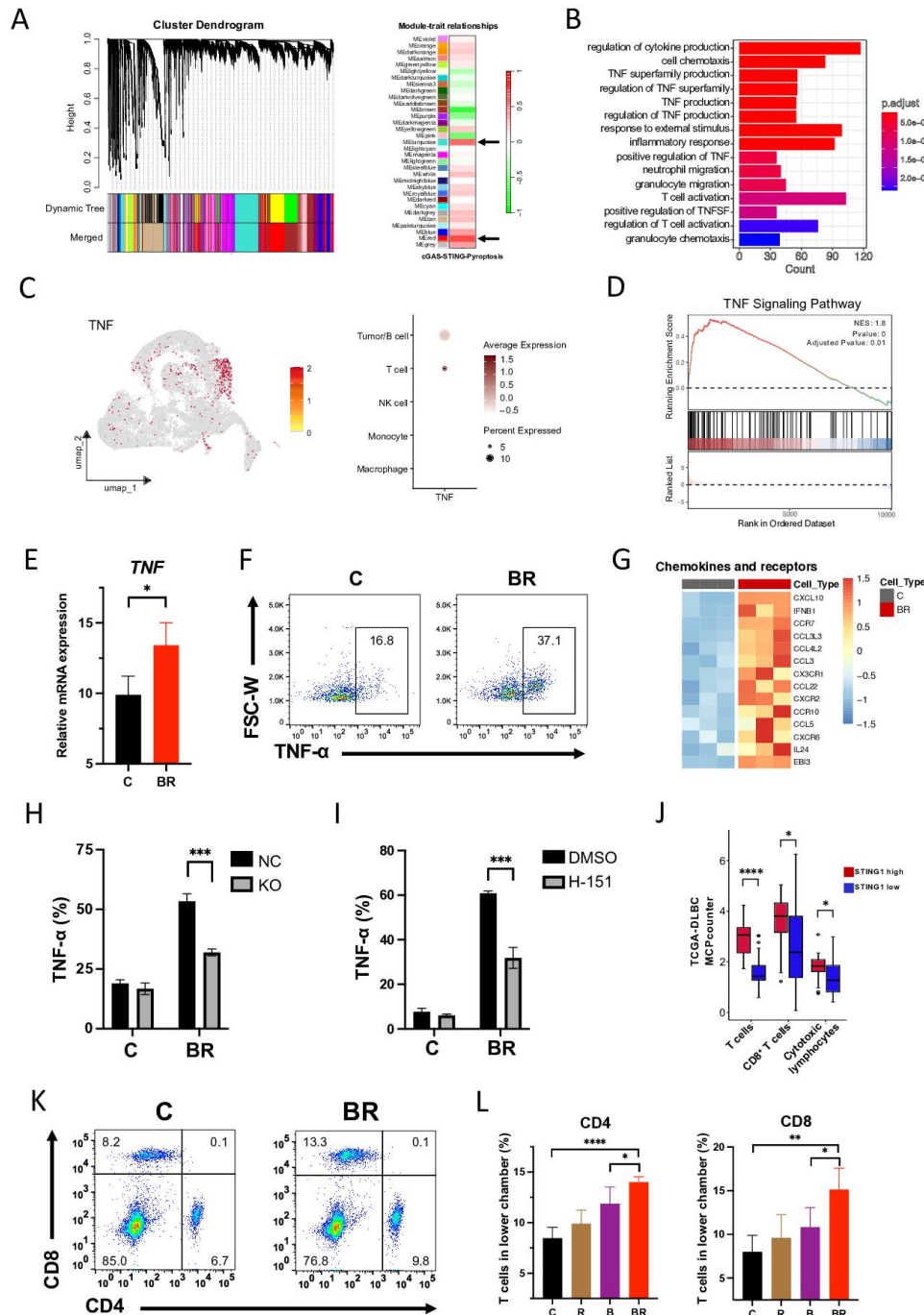
**Figure 5** BR-induced inflammatory microenvironment and T-cell infiltration. (A) WGCNA module identification and correlation analysis. Gene clustering dendrogram and correlation heatmap identifying WGCNA modules in the GDC-DLBCL-2018 cohort. The colors red and green indicate positive and negative correlations, respectively, between the cGAS–STING-pyroptosis signature and module gene expression. Black arrows indicate the two most correlated modules. (B) Signaling pathways enriched in the turquoise and red modules, pathways were obtained from the GO dataset. (C) UMAP plot and DotPlot shows the expression of TNF in the DLBCL scRNA-seq dataset. (D) GSEA results of the TNF signaling pathway (BR vs C). (E) TNF expression assessed by q-PCR. (F) Flow cytometry analysis of TNF-$\alpha$ levels in OCI-LY1 cells. (G) Heatmap depicting the expression of chemokines and receptors in BR-treated relative to untreated cells. (H) Flow cytometry analysis of TNF-$\alpha$ levels in NC OCI-LY1 cells and STING1 KO OCI-LY1 cells. (I) Flow cytometry analysis of TNF-$\alpha$ levels in DMSO and H-151 treated OCI-LY1 cells. (J) Illustrating T-cell infiltration in STING1 high and STING1 low tumors in the TCGA-GDC cohort. (K) Flow cytometry analysis of the proportion of CD4$^+$ and CD8$^+$ T cells migrating toward the lower chamber of the transwell experiment. OCI-LY1 cells pretreated with C, R, B, BR as the lower chamber and T cells was seeded into the upper wells. Corresponding drug of C, R, B, BR was added into the medium during the transwell experiment. (L) Statistical results of the proportion of CD4$^+$ and CD8$^+$ T cells migrating toward tumor cells in the transwell experiment. NC: OCI-LY1 with empty vector, STING1 KO: STING1 Knockout OCI-LY1. C, untreated. R, rituximab monotherapy. B, bendamustine monotherapy. BR, bendamustine plus rituximab combination therapy. *p<0.05; **p<0.01; ***p<0.001; ****p<0.0001. WGCNA, weighted gene co-expression network analysis

receptors in the BR-treated group (figure 5E–G). To understand whether upregulation of inflammatory cytokines is mediated by cGAS–STING pathway, we examined changes of TNF-α expression in STING-downregulated DLBCL cells. TNF-α expression induced by BR was decreased after STING KO (figure 5H) or inhibited by the STING inhibitor H-151 (figure 5I). Above results suggested that BR treatment may induce an immunologically hot tumor microenvironment to facilitate the recruitment of immune cells by activating cGAS–STING and subsequently upregulating proinflammatory factors. To validate this hypothesis, we initially examined the correlation between STING expression and immune cell infiltration within the DLBCL tumors. As shown in figure 5J, patients with high STING expression exhibited elevated T-cell infiltration in their tumors. Since T cells were exposed to bendamustine in our next system, we investigated whether T-cell function would be impaired by the drug. As shown in online supplemental figure S4B, bendamustine was indeed toxic to T cells. Consistently, BR-treated DLBCL cells exhibited an increased ability to recruit T cells when bendamustine was removed prior to coculture with T cells (online supplemental figure S4C). These results suggest that while BR treatment can create an immunologically active tumor microenvironment, even bendamustine does exert some toxic effects on T cells (figure 5K, L and online supplemental figure S4A).

### Enhanced T-cell activation and anti-tumor function by BR therapy

The WGCNA identified a coexpression module associated with cGAS–STING enriched in the T-cell activation pathway (figure 5B). Previous studies have reported that cGAS–STING, as part of the innate immune pathway, can activate adaptive immunity, particularly the immune response of T cells.[38] Hence, we inquired whether the antitumor functionality of T cells could be enhanced after BR treatment in DLBCL. As shown in figure 6A, B, IFN-γ production by T cells was increased in the direct coculture with DLBCL cells in corresponding supernatant of rituximab, bendamustine and BR groups compared with control group, but were not increased when cultured in DLBCL cell supernatant only. There is a synergistically significant increase in BR combination compared with single treatment. Bendamustine treatment had no inhibitory effect on IFN-γ secretion by T cells, excluding toxic influence of bendamustine on T cells (online supplemental figure S4D). Consistently, T cells cocultured with BR-treated tumor cells exhibited stronger activation marker expression such as CD69 and TIM3 (figure 6C, D), which further demonstrated the elevated T cell activation ability of BR-treated DLBCL cells. This increased T-cell activation was specifically observed in direct coculture, emphasizing the critical role of cell surface molecules in DLBCL cells. Direct interaction between T cells and tumor cells involves mutual recognition and binding of MHC molecules on tumor cells and TCR molecules on T cells.[39 40] The abundance of MHC molecules on tumor cells can significantly influence the recognition and activation of T cells.[41] Additionally, previous studies have reported that activation of the STING-IFN-I signaling can upregulate the expression of MHC molecules on the surface of tumor cells.[42] Comparing BR-treated and control tumors revealed increased expression of MHC molecules and costimulatory molecules (figure 6E). Flow cytometry confirmed the upregulation of MHC class I and II molecules at the protein level (figure 6F–I). BR treatment thus enhances T-cell activation and effector function by upregulating MHC molecules in DLBCL cells. Combining BR treatment with T-cell coculture resulted in a near-complete killing effect on DLBCL cells (figure 6J), consistent with the significant clinical efficacy of BR therapy.

Our study demonstrates that BR therapy targets a critical set of genes (online supplemental table 3) that facilitate the shift from innate immunity to adaptive immunity, thereby enhancing antitumor responses. Notably, compiling these genes into a gene set has proven to be a reliable predictor of patient prognosis (online supplemental figure S5A), underscoring the significant potential of BR therapy as a promising treatment option for DLBCL.

### DISCUSSION

DLBCL is a curable disease with the frontline treatment of R-CHOP.[43] However, a subset of patients, particularly the elderly with chronic heart conditions, cannot tolerate the CHOP regimen due to its cardiotoxicity. To understand the potential effectiveness of bendamustine in combination with rituximab, particularly in patients who may not tolerate the standard R-CHOP regimen, we included clinical anecdotes of three elderly patients with DLBCL treated with BR therapy. These cases, along with the scans, highlight the practical and real-world applicability of our findings. The observed favorable and well-tolerated effects of BR therapy on elderly patients with DLBCL emphasize the importance of unraveling its underlying mechanisms. Our investigation reveals that BR treatment induces pyroptosis in DLBCL cells through a cGAS–STING-dependent pathway, eliciting a subsequent immune-activating response.

In clinical practice, even a single cytotoxic agent like bendamustine can have therapeutic effects on elderly patients with DLBCL.[44] This may be explained by our study, which shows that bendamustine has both direct cytotoxic and immunologic effects, further enhanced by rituximab's ability to facilitate immune-mediated cytotoxicity. However, the clinical response to BR therapy may vary, depending to an undefined degree on the patients' T-cell immunity.[45 46] Effective T-cell responses may be critical for the full therapeutic benefit of BR therapy, as our study suggests that the activation of the cGAS–STING pathway and subsequent immune activation play significant roles in the antitumor effects observed. In patients with compromised T-cell function, the efficacy of BR
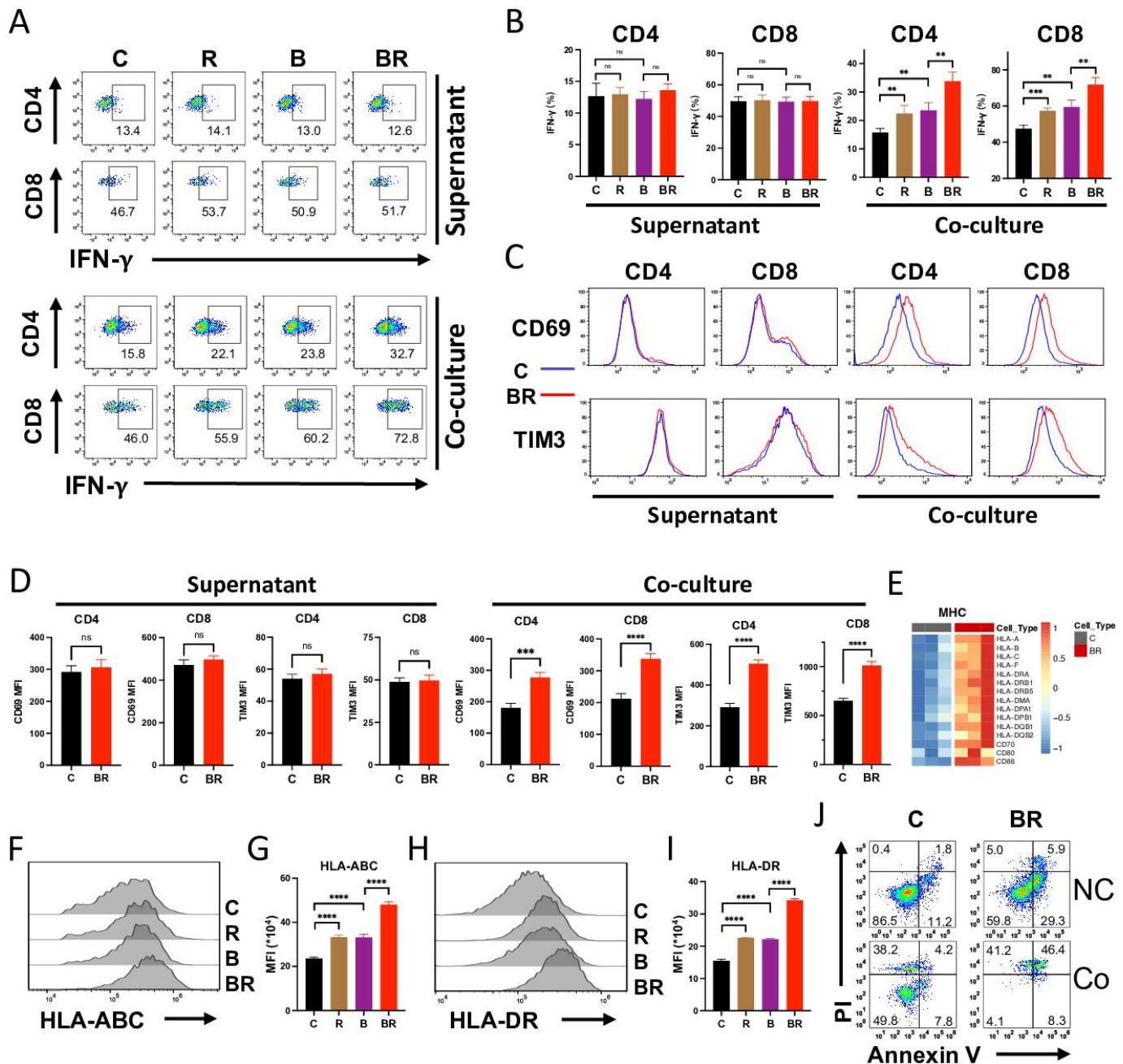
**Figure 6** Enhanced T-cell activation and antitumor function by BR therapy. (A) Flow cytometry was used to assess the expression levels of IFN-γ in CD4+ and CD8+ T cells in coculture model and a supernatant-cultured model. (B) Bar graphs illustrate the levels of IFN-γ in CD4+ and CD8+ T cells in coculture model and a supernatant-cultured model. (C) Flow cytometry analysis was conducted to measure the levels of CD69 and TIM3 in CD4+ and CD8+ T cells in coculture model and a supernatant-cultured model. (D) Bar graphs depict the levels of CD69 and TIM3 in CD4+ and CD8+ T cells in coculture model and a supernatant-cultured model. (E) A heatmap displays genes significantly altered in MHC-related genes in cells treated with BR relative to untreated cells. (F, G) Flow cytometry was used to assess the levels of MHC class I molecules in OCI-LY1 cells. (H, I) Flow cytometry analysis was performed to measure the levels of MHC class II molecules in OCI-LY1 cells. (J) Flow cytometry analysis was conducted to measure the apoptosis levels in OCI-LY1 cells cocultured with T cells and OCI-LY1 cells not cocultured with T cells. Coculture model: diluted 1 volume of T cell to 10 volumes of tumor pretreatment supernatant containing drug of C, R, B, BR, and tumor cell. Then tumor cell and T cell were cocultured for 36 hours. supernatant-cultured model: tumor pretreatment supernatant used to culture T cell for 36 hours. C, untreated. R, rituximab monotherapy. B, bendamustine monotherapy. BR, bendamustine plus rituximab combination therapy. *p<0.05; **p<0.01; ***p<0.001; ****p<0.0001. MHC, major histocompatibility complex.

therapy might be diminished, highlighting the need for personalized treatment strategies based on the immunologic status of each patient.

Bendamustine, recognized for its ability to induce cancer cell death by mediating DNA cross-linking and damage, manifests direct apoptotic and cell cycle

A
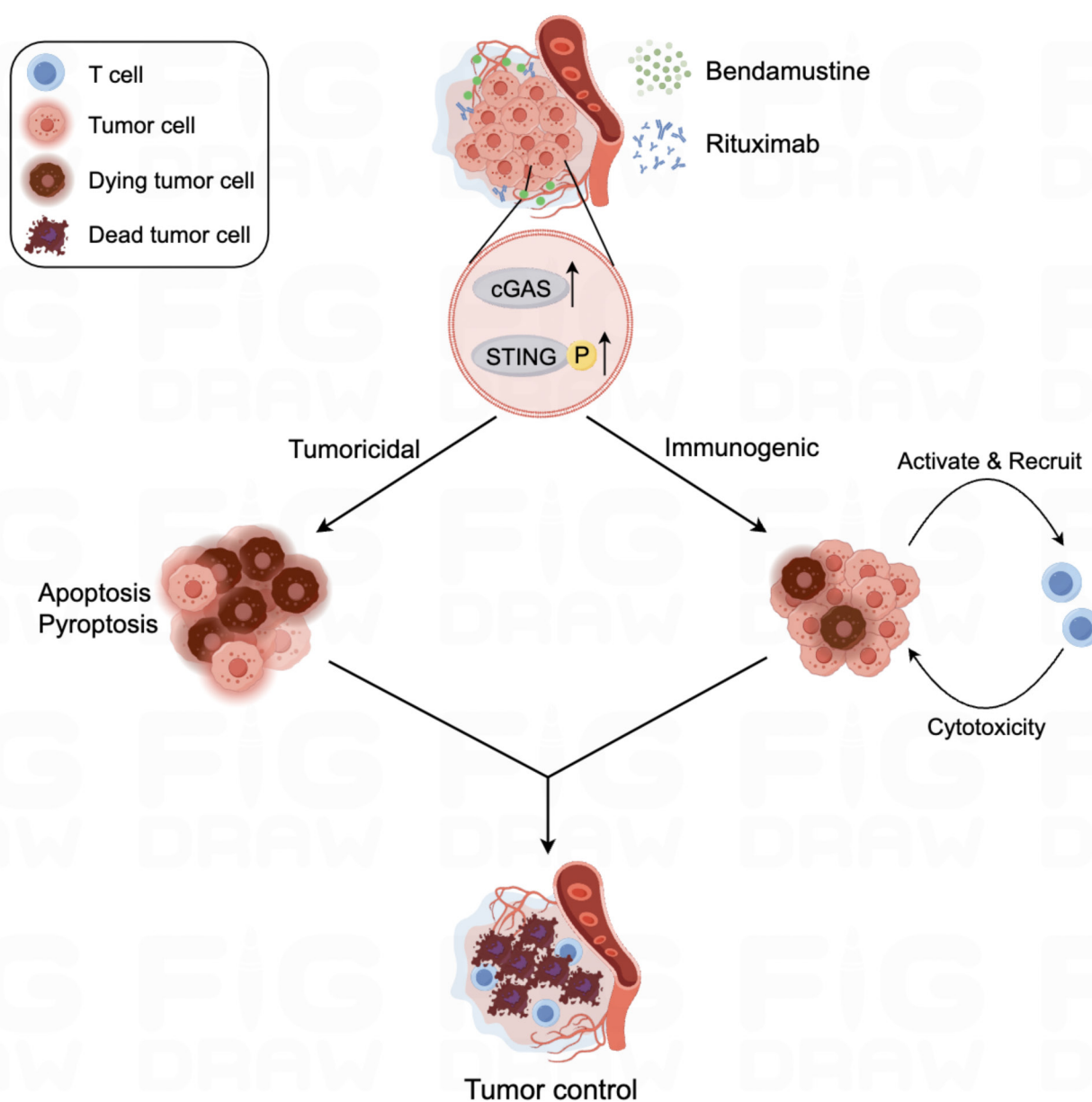


**Figure 7** A schematic mechanism describing the antitumor function by BR therapy. (A) Schematic mechanism describing direct tumoricidal effects and immunomodulatory properties of BR. BR, bendamustine–rituximab.

arrest effects in DLBCL cells. These effects are further enhanced when combined with rituximab, emphasizing the complementary actions of these agents. In vivo, antibody-dependent cellular cytotoxicity of rituximab is complement-dependent,[29 30] as substantiated by the observed synergistic killing effect when complement was added during BR treatment. This elucidates the fundamental mechanism through which BR therapy exerts direct tumoricidal effects on DLBCL cells. Moreover, the transition from apoptosis to pyroptosis during BR incubation suggests a broader therapeutic impact, potentially leveraging the immune system to control tumor growth,

as pyroptosis has been recognized for its potential to stimulate the immune system and enhance cancer immunotherapy efficacy.[47 48]

Although the cGAS–STING pathway exhibits dual roles in tumorigenesis and tumor prevention,[49 50] its specific function in DLBCL remains incompletely understood. Our study illuminates an upregulation of the cGAS–STING pathway with BR treatment, contributing to increased apoptosis and subsequent pyroptosis in DLBCL cells. Both bendamustine and rituximab independently upregulate cGAS and phosphorylated STING1, with a synergistic increase under combination conditions. This

pathway, crucial for intrinsic immunity, surveils aberrant DNA presence in the cytoplasm.[15] While the specific mechanisms of aberrant DNA production in DLBCL cells were not detailed in our study, hypotheses suggest that internal biochemical changes induced by BR therapy, such as DNA cross-linking by bendamustine, may result in abnormal DNA production.[7] Alternatively, cellular stress might trigger the release of mitochondrial DNA, activating the cGAS–STING pathway[51 52]—hypotheses that warrant validation in future studies.

In addition to direct and complement-dependent cytotoxicity, rituximab's elimination of tumor cells involves various immune cell-mediated mechanisms.[53 54] The intrinsic cGAS–STING pathway within tumors can activate immune responses in vivo. The remarkable therapeutic efficacy of BR therapy in patients with DLBCL, coupled with in vitro evidence of BR treatment recruiting and enhancing T-cell effector functions, supports the plausible involvement of immune system activation in BR therapy. While limitations in animal models hinder the precise elucidation of the immune response activated by BR therapy, our in vitro experiments emphasize BR's potential to improve both the quantity and quality of T cells within the DLBCL tumor microenvironment.

Within the tumor microenvironment, inflammatory factors and chemokines play pivotal roles in T-cell recruitment. Activation of the STING pathway by BR therapy facilitates the release of type I interferon, bridging intrinsic and adaptive immune responses.[55 56] Pyroptosis further contributes to this immune-activating effect by releasing inflammatory factors.[57] Our results affirm the upregulation of TNF and CXCL10 in DLBCL cells, endorsing their role in recruiting T cells into the tumor microenvironment. Importantly, BR-induced upregulation of MHC molecules on DLBCL tumor cells enhances their ability to act as antigen-presenting cells, thereby amplifying antitumor immunity.

Mechanistically, BR therapy activates the intrinsic cGAS–STING pathway, inducing apoptosis and pyroptosis in DLBCL cells for direct tumoricidal effects. Simultaneously, BR treatment shapes an immunologically active tumor microenvironment, releasing inflammatory factors and upregulating MHC molecule expression, thereby facilitating T-cell recruitment and activation (figure 7A). This immunomodulatory effect positions BR therapy as a promising candidate for combination with immunotherapy, offering comprehensive insights for refining therapeutic strategies and personalizing treatment in DLBCL.

## Author affiliations

[1]Department of Biochemistry and Molecular Biology, School of Basic Medical Sciences, Guangdong Provincial Key Laboratory of Single Cell Technology and Application, Southern Medical University, Guangzhou, Guangdong, China
[2]Department of General Surgery, Nanfang Hospital, Southern Medical University, Guangzhou, Guangdong, China
[3]Department of Urology, Zhujiang Hospital, Southern Medical University, Guangzhou, Guangdong, China
[4]Department of Hematology, Nanfang Hospital, Southern Medical University, Guangzhou, Guangdong, China

**ORCID iDs**
Ruipei Xiao http://orcid.org/0009-0009-6998-3651
Enguang Bi http://orcid.org/0000-0003-0850-8135

## REFERENCES

1 Miao Y, Medeiros LJ, Li Y, *et al*. Genetic alterations and their clinical implications in DLBCL. *Nat Rev Clin Oncol* 2019;16:634–52.
2 Pfreundschuh M, Schubert J, Ziepert M, *et al*. Six versus eight cycles of bi-weekly CHOP-14 with or without rituximab in elderly patients with aggressive CD20+ B-cell lymphomas: a randomised controlled trial (RICOVER-60). *Lancet Oncol* 2008;9:105–16.
3 Poletto S, Novo M, Paruzzo L, *et al*. Treatment strategies for patients with diffuse large B-cell lymphoma. *Cancer Treat Rev* 2022;110:102443.
4 Sehn LH, Salles G. Diffuse Large B-Cell Lymphoma. *N Engl J Med* 2021;384:842–58.
5 Sarkozy C, Coiffier B. Diffuse large B-cell lymphoma in the elderly: a review of potential difficulties. *Clin Cancer Res* 2013;19:1660–9.

6 Upshaw JN, Nelson J, Rodday AM, *et al*. Association of Preexisting Heart Failure With Outcomes in Older Patients With Diffuse Large B-Cell Lymphoma. *JAMA Cardiol* 2023;8:453–61.

7 Cheson BD, Rummel MJ. Bendamustine: rebirth of an old drug. *J Clin Oncol* 2009;27:1492–501.

8 Hoy SM. Bendamustine: a review of its use in the management of chronic lymphocytic leukaemia, rituximab-refractory indolent non-Hodgkin's lymphoma and multiple myeloma. *Drugs (Abingdon Engl)* 2012;72:1929–50.

9 Rummel MJ, Niederle N, Maschmeyer G, *et al*. Bendamustine plus rituximab versus CHOP plus rituximab as first-line treatment for patients with indolent and mantle-cell lymphomas: an open-label, multicentre, randomised, phase 3 non-inferiority trial. *Lancet* 2013;381:1203–10.

10 Flinn IW, van der Jagt R, Kahl B, *et al*. First-Line Treatment of Patients With Indolent Non-Hodgkin Lymphoma or Mantle-Cell Lymphoma With Bendamustine Plus Rituximab Versus R-CHOP or R-CVP: Results of the BRIGHT 5-Year Follow-Up Study. *JCO* 2019;37:984–91.

11 Ohmachi K, Niitsu N, Uchida T, *et al*. Multicenter phase II study of bendamustine plus rituximab in patients with relapsed or refractory diffuse large B-cell lymphoma. *J Clin Oncol* 2013;31:2103–9.

12 Storti S, Spina M, Pesce EA, *et al*. Rituximab plus bendamustine as front-line treatment in frail elderly (>70 years) patients with diffuse large B-cell non-Hodgkin lymphoma: a phase II multicenter study of the *Fondazione Italiana Linfomi Haematologica* 2018;103:1345–50.

13 Weidmann E, Neumann A, Fauth F, *et al*. Phase II study of bendamustine in combination with rituximab as first-line treatment in patients 80 years or older with aggressive B-cell lymphomas. *Ann Oncol* 2011;22:1839–44.

14 Fu D, Calvo JA, Samson LD. Balancing repair and tolerance of DNA damage caused by alkylating agents. *Nat Rev Cancer* 2012;12:104–20.

15 Hopfner KP, Hornung V. Molecular mechanisms and cellular functions of cGAS-STING signalling. *Nat Rev Mol Cell Biol* 2020;21:501–21.

16 Kwon J, Bakhoum SF. The Cytosolic DNA-Sensing cGAS-STING Pathway in Cancer. *Cancer Discov* 2020;10:26–39.

17 Burdette DL, Monroe KM, Sotelo-Troha K, *et al*. STING is a direct innate immune sensor of cyclic di-GMP. *Nature New Biol* 2011;478:515–8.

18 Sen T, Rodriguez BL, Chen L, *et al*. Targeting DNA Damage Response Promotes Antitumor Immunity through STING-Mediated T-cell Activation in Small Cell Lung Cancer. *Cancer Discov* 2019;9:646–61.

19 Li A, Yi M, Qin S, *et al*. Activating cGAS-STING pathway for the optimal effect of cancer immunotherapy. *J Hematol Oncol* 2019;12:35.

20 Bal E, Kumar R, Hadigol M, *et al*. Super-enhancer hypermutation alters oncogene expression in B cell lymphoma. *Nature New Biol* 2022;607:808–15.

21 Hayman TJ, Baro M, MacNeil T, *et al*. STING enhances cell death through regulation of reactive oxygen species and DNA damage. *Nat Commun* 2021;12:2327.

22 Liu J, Yuan L, Ruan Y, *et al*. Novel CRBN-Recruiting Proteolysis-Targeting Chimeras as Degraders of Stimulator of Interferon Genes with In Vivo Anti-Inflammatory Efficacy. *J Med Chem* 2022;65:6593–611.

23 Macaya I, Roman M, Welch C, *et al*. Signature-driven repurposing of Midostaurin for combination with MEK1/2 and KRASG12C inhibitors in lung cancer. *Nat Commun* 2023;14:6332.

24 Roider T, Seufert J, Uvarovskii A, *et al*. Dissecting intratumour heterogeneity of nodal B-cell lymphomas at the transcriptional, genetic and drug-response levels. *Nat Cell Biol* 2020;22:896–906.

25 Steen CB, Luca BA, Esfahani MS, *et al*. The landscape of tumor cell states and ecosystems in diffuse large B cell lymphoma. *Cancer Cell* 2021;39:1422–37.

26 Schmitz R, Wright GW, Huang DW, *et al*. Genetics and Pathogenesis of Diffuse Large B-Cell Lymphoma. *N Engl J Med* 2018;378:1396–407.

27 Langfelder P, Horvath S. WGCNA: an R package for weighted correlation network analysis. *BMC Bioinformatics* 2008;9:559.

28 Szklarczyk D, Gable AL, Nastou KC, *et al*. The STRING database in 2021: customizable protein-protein networks, and functional characterization of user-uploaded gene/measurement sets. *Nucleic Acids Res* 2021;49:D605–12.

29 Kumar A, Planchais C, Fronzes R, *et al*. Binding mechanisms of therapeutic antibodies to human CD20. *Science* 2020;369:793–9.

30 Rougé L, Chiang N, Steffek M, *et al*. Structure of CD20 in complex with the therapeutic monoclonal antibody rituximab. *Science* 2020;367:1224–30.

31 Gentili M, Liu B, Papanastasiou M, *et al*. ESCRT-dependent STING degradation inhibits steady-state and cGAMP-induced signalling. *Nat Commun* 2023;14:611.

32 Kuchitsu Y, Mukai K, Uematsu R, *et al*. STING signalling is terminated through ESCRT-dependent microautophagy of vesicles originating from recycling endosomes. *Nat Cell Biol* 2023;25:453–66.

33 Zhong B, Zhang L, Lei C, *et al*. The ubiquitin ligase RNF5 regulates antiviral responses by mediating degradation of the adaptor protein MITA. *Immunity* 2009;30:397–407.

34 Yang B, Liu Y, Cui Y, *et al*. RNF90 negatively regulates cellular antiviral responses by targeting MITA for degradation. *PLoS Pathog* 2020;16:e1008387.

35 Shi X, Yang Y, Zhang W, *et al*. FLASH X-ray spares intestinal crypts from pyroptosis initiated by cGAS-STING activation upon radioimmunotherapy. *Proc Natl Acad Sci U S A* 2022;119:e2208506119.

36 Zhang W, Li G, Luo R, *et al*. Cytosolic escape of mitochondrial DNA triggers cGAS-STING-NLRP3 axis-dependent nucleus pulposus cell pyroptosis. *Exp Mol Med* 2022;54:129–42.

37 Balkwill F. Tumour necrosis factor and cancer. *Nat Rev Cancer* 2009;9:361–71.

38 Cao LL, Kagan JC. Targeting innate immune pathways for cancer immunotherapy. *Immunity* 2023;56:S1074-7613(23)00331-X:2206–17:.

39 He Q, Jiang X, Zhou X, *et al*. Targeting cancers through TCR-peptide/MHC interactions. *J Hematol Oncol* 2019;12:139.

40 Zareie P, Szeto C, Farenc C, *et al*. Canonical T cell receptor docking on peptide-MHC is essential for T cell signaling. *Science* 2021;372:eabe9124.

41 Chen X, Lu Q, Zhou H, *et al*. A membrane-associated MHC-I inhibitory axis for cancer immune evasion. *Cell* 2023;186:3903–20.

42 Lv J, Wei Y, Yin J-H, *et al*. The tumor immune microenvironment of nasopharyngeal carcinoma after gemcitabine plus cisplatin treatment. *Nat Med* 2023;29:1424–36.

43 Lugtenburg PJ, Mutsaers PGNJ. How I treat older patients with DLBCL in the frontline setting. *Blood* 2023;141:2566–75.

44 Berglund A, Molin D, Larsson A, *et al*. Tumour markers as early predictors of response to chemotherapy in advanced colorectal carcinoma. *Ann Oncol* 2002;13:1430–7.

45 Leoni LM, Bailey B, Reifert J, *et al*. Bendamustine (Treanda) displays a distinct pattern of cytotoxicity and unique mechanistic features compared with other alkylating agents. *Clin Cancer Res* 2008;14:309–17.

46 Friedberg JW. Relapsed/refractory diffuse large B-cell lymphoma. *Hematology Am Soc Hematol Educ Program* 2011;2011:498–505.

47 Wang X, Li Y, Hasrat K, *et al*. Sequence-Responsive Multifunctional Supramolecular Nanomicelles Act on the Regression of TNBC and Its Lung Metastasis via Synergic Pyroptosis-Mediated Immune Activation. *Small* 2023;19.

48 Li F, Zhang X-Q, Ho W, *et al*. mRNA lipid nanoparticle-mediated pyroptosis sensitizes immunologically cold tumors to checkpoint immunotherapy. *Nat Commun* 2023;14:4223.

49 Kwon M, Leibowitz ML, Lee JH. Small but mighty: the causes and consequences of micronucleus rupture. *Exp Mol Med* 2020;52:1777–86.

50 Bakhoum SF, Ngo B, Laughney AM, *et al*. Chromosomal instability drives metastasis through a cytosolic DNA response. *Nature New Biol* 2018;553:467–72.

51 Zecchini V, Paupe V, Herranz-Montoya I, *et al*. Fumarate induces vesicular release of mtDNA to drive innate immunity. *Nature New Biol* 2023;615:499–506.

52 Hu MM, Shu HB. Mitochondrial DNA-triggered innate immune response: mechanisms and diseases. *Cell Mol Immunol* 2023;20:1403–12.

53 Smith MR. Rituximab (monoclonal anti-CD20 antibody): mechanisms of action and resistance. *Oncogene* 2003;22:7359–68.

54 Clynes RA, Towers TL, Presta LG, *et al*. Inhibitory Fc receptors modulate in vivo cytotoxicity against tumor targets. *Nat Med* 2000;6:443–6.

55 Zitvogel L, Galluzzi L, Kepp O, *et al*. Type I interferons in anticancer immunity. *Nat Rev Immunol* 2015;15:405–14.

56 Liang Y, Hannan R, Fu YX. Type I IFN Activating Type I Dendritic Cells for Antitumor Immunity. *Clin Cancer Res* 2021;27:3818–24.

57 Wei X, Xie F, Zhou X, *et al*. Role of pyroptosis in inflammation and cancer. *Cell Mol Immunol* 2022;19:971–92.